Additive Manufacturing Letters 14 (2025) 100302

Contents lists available at ScienceDirect

Additive Manufacturing Letters

journal homepage: www.elsevier.com/locate/addlet

Short communication

Combining fusion-based and solid-state additive manufacturing: Investigation of additive DED structures with friction surfacing interlayer

Zina Kallien [a,c,*], Eloise Eimer [b], Arne Roos [a], Victor Ortolland [b], Lars Rath [a], Stewart Williams [b], Benjamin Klusemann [a,c]

[a] Helmholtz-Zentrum Hereon, Institute of Material and Process Design, Solid State Materials Processing, Max-Planck-Straße 1, 21502 Geesthacht, Germany
[b] Cranfield University, Welding and Additive Manufacturing Centre, Bedford MK43 0AL, United Kingdom
[c] Leuphana University Lüneburg, Institute for Production Technology and Systems, Universitätsallee 1, 21335, Lüneburg, Germany

ARTICLE INFO

Keywords:
WAAM
Friction surfacing
Dissimilar aluminium alloys
Interface
Micro-flat tensile testing

ABSTRACT

Fusion-based additive manufacturing (AM) techniques face some challenges for aluminium due to the necessity of material melting resulting in insufficient bonding. The present work provides a novel insight into the combination of fusion-based and solid-state AM approaches to successfully generate structures from different aluminium alloys. Specifically, the friction-based solid-state AM technique of friction surfacing (FS) is used to generate an interlayer structure on AA2050 substrate material. On top of this structure, additional AA5087 is deposited via Wire and Arc Additive Manufacturing (WAAM). For the FS interlayer structure, two different alloys, AA5083 and AA7050, are explored. Additionally, the effect of inter-layer rolling is investigated for the final WAAM structure. The built structures are investigated with special focus on the interfaces, i.e., FS deposit-to-substrate and WAAM deposit-to-FS deposit interfaces. In the cross sections, no defects could be detected at the FS deposit-to-substrate interfaces and the structures did not show visible cracks at the WAAM deposit-to-FS deposit interfaces. The investigation showed that the mechanical properties of the WAAM structure improve when inter-layer rolling is applied, leading to homogeneous mechanical properties across the interfaces. The study highlights that FS as friction-based solid-state AM process is capable to build interlayer structures for material combinations, which cannot be achieved directly via a fusion-based process. The approach of combining different AM techniques can be advantageous not only to achieve a dissimilar material combinations but also to build hybrid structures with locally optimized properties.

1. Introduction

The layer-by-layer manufacturing of a structure, known as Additive Manufacturing (AM), has received much attention by research and industry in the last decades, especially to produce lightweight structures [1]. Various metallic materials can be processed [2], where the most common approaches are based on material melting and solidification in order to build the desired structure [3]. For lightweight structures, aluminium alloys are widely used due to their high strength-to-density ratio. Aluminium–lithium alloys are a relatively recent alloy family that possess higher Young's modulus and strength as well as lower density than other alloys [4]. Although aluminium–lithium AM research has been conducted [5–8], it is not mature enough for industrial implementation yet.

The combination of conventional forming, such as casting or forging, with AM is a hybrid manufacturing approach that takes advantage of both traditional and AM capabilities [9–11]. This can enable the use of alloys, such as aluminium–lithium, that can be challenging for a deposition via AM. AM enables high geometrical flexibility, resulting in the capability of producing geometries close to the final product, leading to waste reduction compared to subtractive manufacturing. However, building large components can be lengthy and the benefits of AM are often suboptimal when manufacturing simple geometrical features. Therefore, the combination of both processes can also lead to sustainable manufacturing of efficient designs with the potential to produce multi-material structures. Wire and Arc Additive Manufacturing (WAAM) is a wire-based Directed Energy Deposition (DED) AM technology that operates in open architecture without the need for an inert or vacuum atmosphere. It also has a relatively high deposition rate compared with other metal AM processes [12]. Therefore, it is particularly suitable for hybrid manufacturing.

* Corresponding author at: Helmholtz-Zentrum Hereon, Institute of Material and Process Design, Solid State Materials Processing, Max-Planck-Straße 1, 21502 Geesthacht, Germany.
E-mail address: zina.kallien@hereon.de (Z. Kallien).

https://doi.org/10.1016/j.addlet.2025.100302
Received 17 June 2025; Received in revised form 10 July 2025; Accepted 11 July 2025
Available online 23 July 2025

When compatible alloys are used, the wrought and AM material interface performs well [13–15]. However, the joint between wrought products and WAAM material can suffer from defects similar to those found in fusion welding joints. Eimer et al. [13,14] studied the microstructure and mechanical properties of the interface between aluminium rolled plates and WAAM deposits. The investigation of an AA2050 plate with AA2319 WAAM deposit combination showed a high porosity level at the fusion zone and a softening of the plate in the heat-affected zone. The authors pointed out similarities between the detrimental phenomena occurring during fusion welding and the deposition of the first AM layer on a substrate via a fusion-based approach. These welding challenges have been widely reported for aluminium–lithium alloys. A high porosity level is often observed in aluminium–lithium fusion welds, as the lithium increases the molten pool reactivity with oxygen, promoting the formation of an oxide layer that increases hydrogen absorption and prevents gas pores from escaping during solidification [16]. These phenomena have been reported since the 70's [17] and are still being investigated now [18]. Cracking can also occur during the fusion welding of aluminium–lithium alloys when their chemical composition generates a solidification path prone to eutectic formation [16]. Therefore, the addition of WAAM features directly onto aluminium–lithium plates is fundamentally challenging. Solid state welding is often used to overcome these fusion welding challenges, and defect-free aluminium–lithium joints can be produced via Friction Stir Welding [19,20]. Solid-state processed materials could therefore be a solution as an interlayer structure between a wrought aluminium–lithium substrate and a WAAM structure.

Additionally, friction-stir based methods have been used for the inter-layer processing of fusion-based AM structures. For instance, friction stir processing (FSP) was shown to enhance the mechanical properties of additive structures [21,22]. Due to the nature of these approaches, friction stir-based solid state layer deposition techniques are also highly interesting for building interlayer structures. Solid-state layer deposition processes like friction surfacing (FS) operate below the materials melting temperature and the layer deposition is enabled via friction and plastic deformation. This approach allows the deposition of various similar and dissimilar metallic materials, for instance, titanium alloys [23], aluminium alloys [24], Inconel [25] or steels [26]. A distinct feature of solid-state layer deposition processes is the ability to join metals with physically and metallurgically very different properties, such as aluminium onto steel [27]. The FS technique has some drawbacks such as being a discontinuous process [28] applicable to a limited range of geometry in 2.5 dimensions. It is also difficult to produce small FS features. Despite these limitations, the technique has large potential to build an interlayer structure, i.e., achieve the critical material combination via FS and continue the deposition with a fusion-based process afterwards. To the best knowledge of the authors, there is no research study available that systematically investigates the combination of FS structures with a fusion-based AM approach.

This study aims to determine the capabilities of multi-layer friction surfacing (MLFS) to build an interlayer structure between an aluminium–lithium plate and a WAAM deposit to overcome the challenges mentioned above. For this investigation, AA2050 was chosen as the substrate material due to its high potential in the aircraft industry [29]. Moreover, previous studies reported successful FS layer deposition of AA5083 on AA2050 substrates [30,31]. AA5087 was selected as the WAAM alloy as its strength can be significantly improved by rolling [32] as opposed to 2000 series alloys that require a heat treatment. Two different aluminium alloys, i.e., AA5083 and AA7050, are included in the investigation for the multi-layer FS structure. AA5083 is expected to show good compatibility with the AA5087 WAAM deposit and AA7050 is a high-strength aluminium alloy, aiming for a high-performing joint. The hybrid structures containing substrate, FS interlayer structure and WAAM structure (WAAM with and without inter-layer rolling), are investigated in detail. A special focus is on the characterization of the interfaces, i.e., FS deposited material-substrate and WAAM deposited material-FS deposited material, with regard to mechanical properties. For that purpose, micro-flat tensile specimens were extracted from these regions of the structure. The results provide valuable insight into the strength of the respective interfaces and the comparison of the different approaches used for hybrid structures. The results underline the potential of FS deposits for interlayer structures for challenging dissimilar material combinations.

2. Materials and methods

2.1. Materials

AA5083 and AA7050 alloys were investigated for the MLFS deposit as interlayer structure between AA2050 substrates and AA5087 WAAM deposit. AA2050-T84 rolled plates (300 mm length, 130 mm width, 12.5 mm thickness) are used as substrates. Fig. 1 presents the schematic of the approach investigated in this study. Table 1 lists the alloys, their temper states, main alloying elements and application during this work. Details on the individual used consumable materials and processes are provided in the following sections.

2.2. Friction surfacing

Friction surfacing (FS) is a solid-state joining process first mentioned 1941 in a patent by Klopstock and Neelands [33]. The FS process can be divided into four steps with two main process phases, i.e., plasticizing and deposition phase. After the stud is positioned above the starting position, a predefined rotational speed and, in case of force controlled operation, an axial force, or a predefined axial feed rate, in case of feed rate controlled operation, is applied. The rotating stud is pressed onto the substrate surface and causes frictional heating at the materials' interface. As a result, the tip of the stud starts to deform and plasticize. The outer part of the stud tip material is pressed outward and starts to form the so called flash [34], which is a characteristic of the FS process. Continuous torque input changes the main heat source from hard body friction to viscoplastic shearing at the interface between the stud tip and the already deposited material in the plasticizing area [35,36]. When this stage is reached, a relative translational movement between substrate and stud is superimposed and enables layer deposition along the programmed path. The deposition ends either by reaching the target coordinates or when the stud is consumed.

The main FS process parameters are rotational speed, axial force or feed rate as well as the travel speed for the relative translational movement. The process parameters determine the energy input and have to be selected in accordance with the materials to be deposited [37]. Furthermore, it is well known that the FS process parameters and resulting temperatures affect the resulting deposit geometry [38].

In the course of this study, a custom-designed friction welding machine (RAS, H. Loitz Robotik, Germany) has been used. The RAS has a vertical spindle system (max. rotational speed up to 6000 rpm) in combination with computer-aided numerical control (CNC) of the machine table (work area 1.5 m $\times$ 0.5 m) in the horizontal plane. The machine has a stiff design and can therefore provide axial forces up to 60 kN without significant deflection. The forces in all spatial directions, the spindle torque as well as displacements are recorded.

For this study, AA5083 H112 and AA7050 T74511 have been used as consumable stud materials (125 mm length, 20 mm diameter). A backing plate of AA2024 T3 (300 mm length, 130 mm width, 8 mm thickness) has been mounted between substrate and worktable. Prior to the first layer deposition, the substrate surface was ground using P100 grit sandpaper [39] and the surface in the FS area has been further cleaned with acetone using a lint-free cloth.

For the AA5083 FS build, all layers were deposited at constant process parameters, as shown in Table 2. Since it is more challenging to achieve sufficient bonding between FS layer and substrate material with AA7050, the parameters had to be adjusted accordingly.

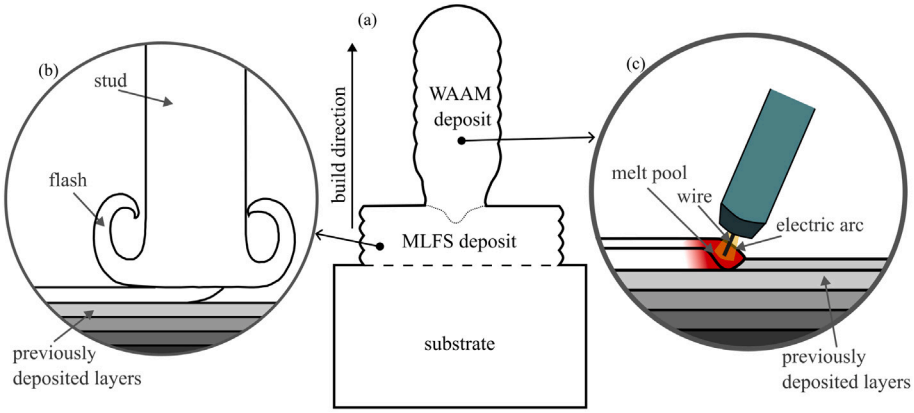

Fig. 1. Schematic illustration of the deposition approach used in this study to create a hybrid structure (a) with multi-layer friction surfacing (MLFS) interlayer structure (b) for Wire and Arc Additive Manufacturing (WAAM) (c).

Table 1
Aluminium alloys used in this study for substrate material, FS and WAAM deposition.

Alloy	Temper state	Alloying elements [wt.%]	Use
AA2050	T84	Cu (3.2–3.9), Li (0.7–1.3), Ag (0.2–0.7),Mg (0.2–0.6), Mn (0.2–0.5), Zr (0.6–0.14)	substrate
AA7050	T74511	Zn (5.7–6.7), Cu (2–2.6), Mg (1.9–2.6)	MLFS deposit
AA5083	H112	Mg (4–4.9), Mn (0.4–1), Cr (0.05–0.25)	MLFS deposit
AA5087	As-deposited and rolled	Mg (4.5–5.2), Mn (0.7–1.1), Cr (0.05–0.25), Zr (0.1–0.2)	WAAM deposit

Table 2
Process parameters for first and subsequent layer deposition via MLFS for AA5083 and AA7050 on AA2050 substrate material.

Material	Layer	Axial force [kN]	Rotational speed [rpm]	Translational speed [mm/s]
AA5083/AA2050	1st, 2nd, …	8	1200	6
AA7050/AA2050	1st 2nd, 3rd, …	12 12	1000 500	8 4

Parameters with higher rotational and translational speed were applied for the first layer to substrate (LTS), i.e., AA7050 on AA2050, deposit, which generate thinner layers but have shown higher bonding strength [40]. Since parameters with lower rotational and translational speed generate thicker layers, these parameters have been applied for the subsequent layers, i.e., AA7050 to AA7050 layer to layer (LTL), to reduce the amount of layers necessary and thus increase productivity in generating the MLFS interlayer structures. After each layer deposition, the build was allowed to cool down to room temperature. The main process parameters used for depositing the different layers are listed in Table 2. The MLFS builds showed a high reproducibility and stable layer deposition behaviour, leading to homogeneous layer geometries and appearance of the stacks, as shown in Fig. 2. For the investigation of the MLFS-substrate interface, nine layers were deposited on top of each other in order to provide sufficient material for tensile specimen extraction. For the final structures with WAAM deposit on top of the MLFS interlayer structure, four layers (AA5083) and five layers (AA7050) were deposited, respectively, to reach a stack height of at least 5 mm.

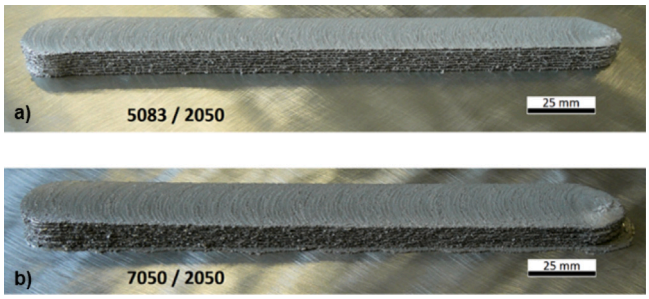

Fig. 2. Dissimilar MLFS builds, showing (a) AA5083 deposited onto AA2050 and (b) AA7050 deposited onto AA2050.

2.3. Wire and Arc Additive Manufacturing

A Fronius CMT Advanced 4000R power source was used with the Cold Metal Transfer (CMT) Pulse C0879 + P synergic line and a 1.2 mm diameter AA5087 commercial wire. With this deposition process, the material transfer occurs via dip transfer and spray mode. The process parameters, identical to those used by Gu et al.[32] in their study of the effect of rolling on AA5087 WAAM are indicated in Table 3. Deposits were made directly on the substrate for references, and on top of the MLFS for the core study. In both cases, the surface was finished using an abrasive disc and cleaned with isopropanol.

The process parameters of the first two layers were adjusted to increase the heat input and compensate for the heat sink due to the

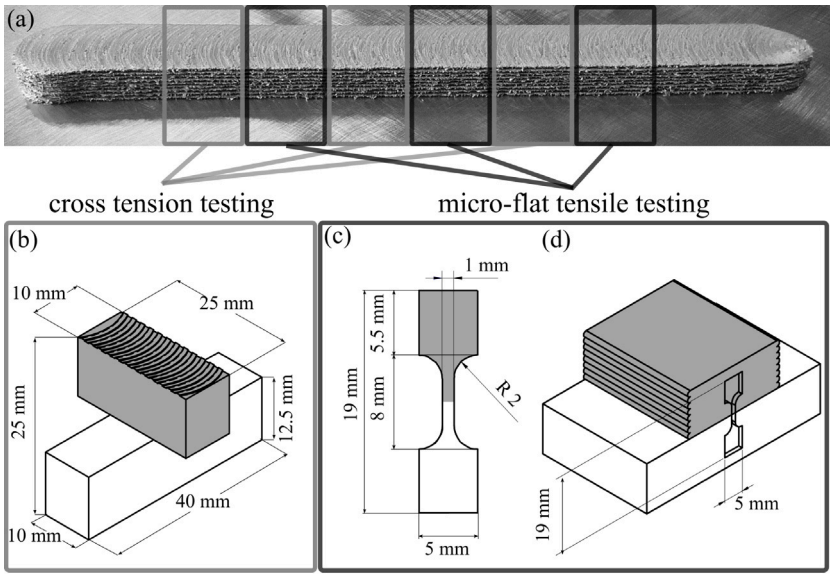

Fig. 3. Samples for testing are extracted along the deposition length from the multi-layer friction surfacing (MLFS) stacks (a) for cross tension testing (CTT) and (b) and micro-flat tensile testing (MFTT) (c, d), as also performed in [31] for AA5083 MLFS deposits.

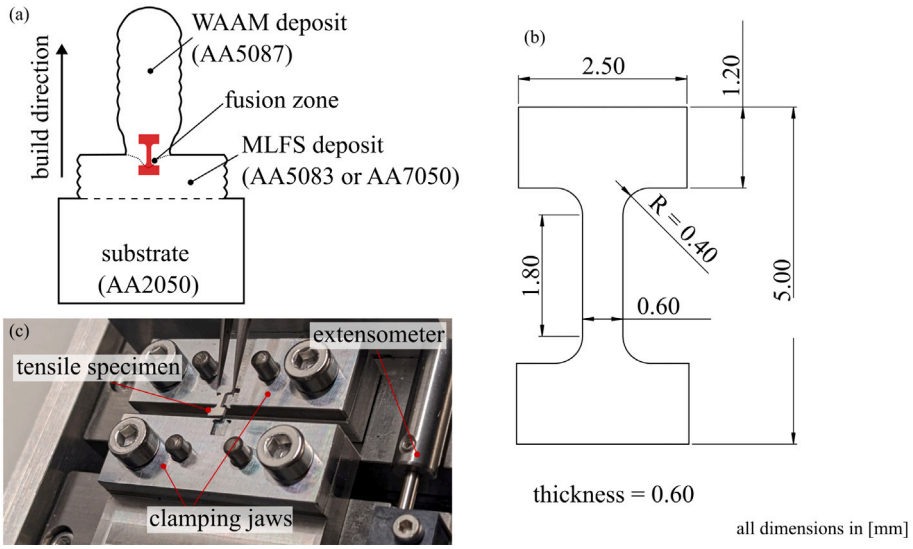

Fig. 4. Schematic overview of the cross section (a) with AA5087 WAAM build deposited onto AA5083 or AA7050 MLFS builds on AA2050 substrates, showing the extraction position of the micro-flat tensile specimens (b). Setup for micro-flat tensile testing with (c) mounting of the specimen in the test stage.

proximity of the substrate. This is a standard method implemented when depositing on a substrate to control the wall base width [13], see Table 3. Using these deposition conditions, a magnesium loss caused by this element's low vaporization point of 0.3wt%, is expected [32]. 150 mm long single bead walls were deposited with alternating start and stop position.

Inter-pass rolling was applied through a 100 mm diameter roller by a hydraulic cylinder as described by Gu et al. [32]. A load of 45 kN and a rolling speed of 10 mm/s were used. Inter-pass rolling was applied between each deposited WAAM layer 30 s after deposition. For both, un-rolled and rolled conditions, 180 s of waiting time was applied between each layer deposition.

Table 3
Process parameters for the deposition of AA5087 via WAAM.

Process parameter	Values
Travel speed	10 mm/s
Wire feed speed [m/min]	Layer 1 and 2 : 7 m/min Layer 3 to 10: 6 m/min
Shielding gas flow rate	20 L/min
Contact to workpiece distance	15 mm
Heat input (layer 3 to 10)	177.9 J/mm [32]

2.4. Sample preparation & metallography

Cross sections of the built structures were prepared following common metallographic practices. Electrochemical etching of the samples was done using Barker's etching solution (15 V, 70 seconds) to reveal the grain structure. The images of the cross section were taken using a light microscope VHX-6000 (Keyence, Germany).

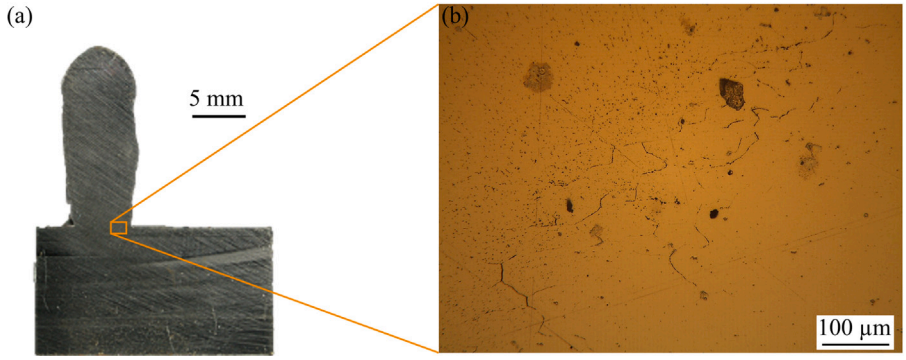

Fig. 5. Micrograph of AA5087 onto AA2050 via WAAM: (a) overview of transverse cut and (b) higher magnification macrograph of the AA5087-AA20250-interface after polishing, clearly showing cracks.

2.5. Mechanical testing

2.5.1. Hardness

Micro-hardness measurements were performed for the cross sections of WAAM-MLFS welds as well as for the MLFS deposits (no WAAM on top) using Durascan 70 G5 (Emco-Test, Austria) automated hardness machine. A Vickers indenter was used applying a load of 200 g, respectively, with a holding time of 10 seconds. The indents were distributed at equidistant spacing of 0.5 mm.

2.5.2. MLFS-substrate interface

Additional MLFS stacks were produced in order to investigate the bonding of the MLFS stack to the substrate, i.e., no additional WAAM was performed. Different samples were used to characterize the bonding via (i) cross tension testing (CTT) and (ii) micro-flat tensile testing (MFTT). Specimens for both testing approaches were extracted along the stacks, leaving a distance of 25 mm to the start and end of the stack, see Fig. 3. The MFTT specimens were extracted perpendicular to the LTS interface plane with approximately 50% of the gauge length inside the MLFS stack material and present a thickness of 1 mm. The MFTT is performed on a 5 kN load cell tensile machine (ZwickRoell, Germany) in displacement control at 0.1 mm/min. The CTT specimen provide a larger gauge section with a testing area of 10 × 10 mm^2. The CTT specimens are tested using a compression test setup using a fork-like tool. The tests were performed on a 100 kN tensile machine (ZwickRoell, Germany) in displacement control at a speed of 0.125 mm/min. The results for AA5083/AA2050 are discussed in detail in a previous study [31] and here just briefly provided for completeness.

2.5.3. WAAM-MLFS interface

MFTT was chosen to quantitatively characterize the WAAM/MLFS interfaces. Via electro discharge machining (EDM), blocks with the contour of the micro-flat tensile specimens perpendicular to the interface with about 50% of the test length within the WAAM as well as the MLFS material respectively, as shown in Fig. 4, were taken from the selected samples. The individual micro-flat specimens were then milled from the EDM blocks.

Micro-flat tensile were tested at a speed of 0.1 mm/min, using a Deben MICROTEST microtensile test stage (Deben UK Ltd, United Kingdom) as depicted in Fig. 4 with the data acquisition software Deben MICROTEST Version 6.3.30 (Deben UK Ltd, United Kingdom). Due to its dimensions and the integrated controller, the system can be used inside confined spaces e.g. underneath an light optical microscope in order to observe microscopic changes on the tested specimens, i.e., local necking.

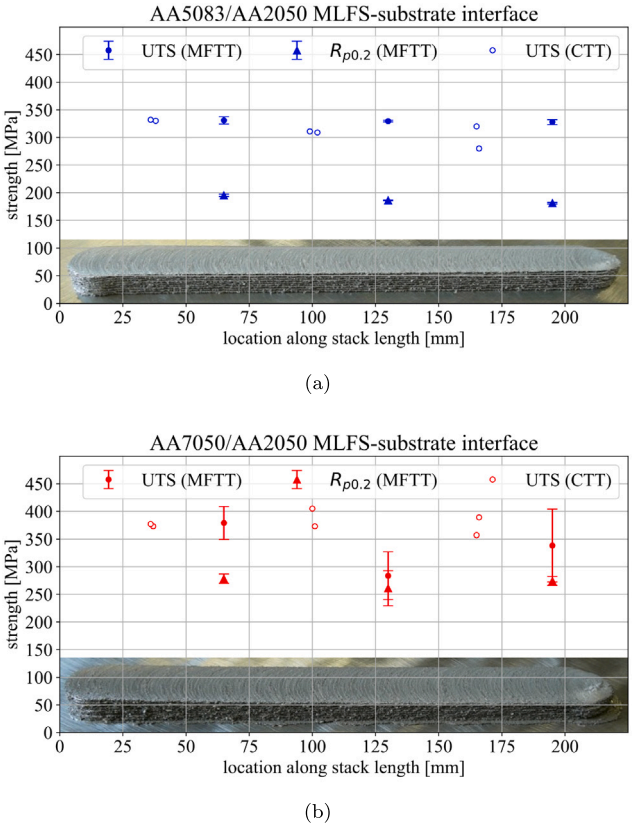

Fig. 6. Results from cross tension testing (CTT) and micro-flat tensile testing (MFTT) for specimens extracted from MLFS stacks built on AA2050 substrates using (a) AA5083 [31] and (b) AA7050 consumable studs. The results of AA5083 (a) were partially adapted from [31].

3. Results

3.1. Reference WAAM sample (without MLFS interlayer layers)

For referencing purposes, AA5087 was deposited directly via WAAM onto the AA2050 substrate. Fig. 5 shows macrographs of the interface, where liquation cracking can be observed. This behaviour is common in the partially melted zone (PMZ) in the root area of dissimilar joints [41], as reported by Hong et al. [42] for AA6061 to AA7075 aluminium resistance spot welding and Huang et al. [43] for gas metal arc welding of AA2024, AA6061 and AA7075 with various filler materials. Since WAAM is a fusion-based approach, these zones are process-characteristic, clearly demonstrating the issue faced when

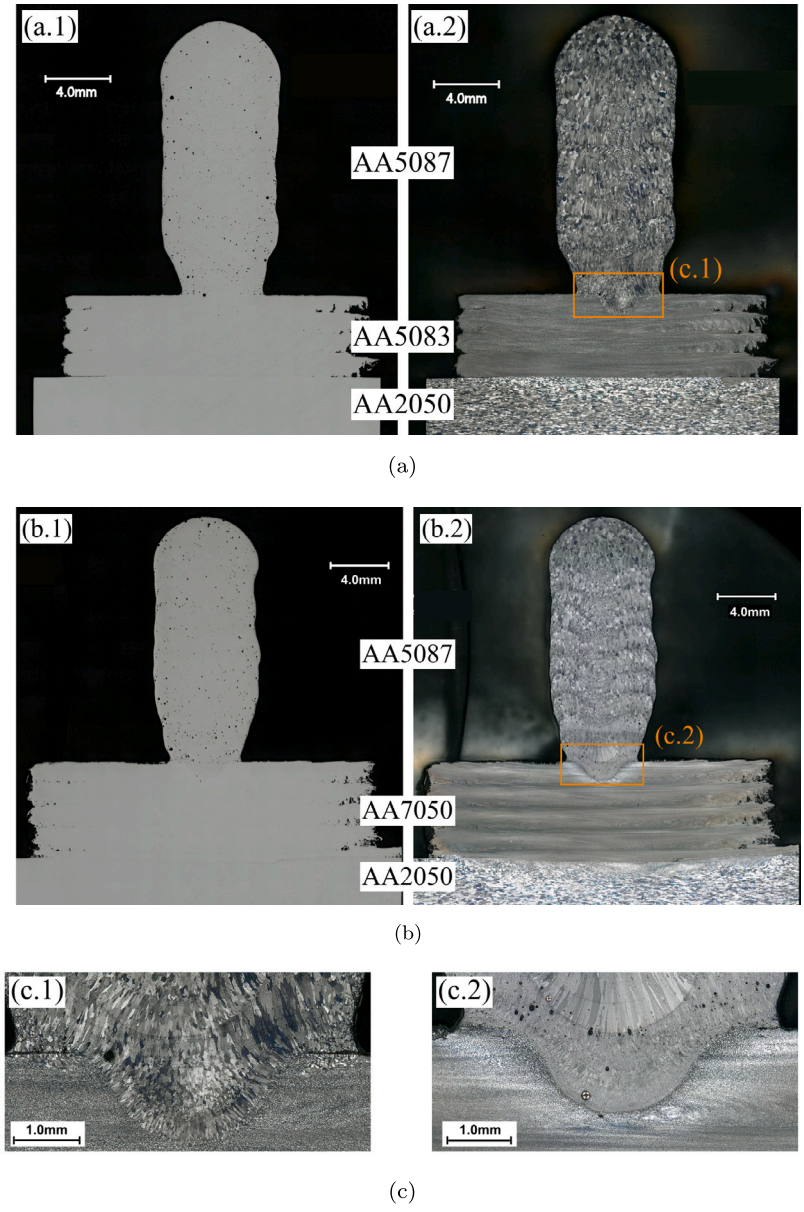

Fig. 7. Cross sections before and after etching for WAAM-MLFS structure on AA2050 substrate with WAAM deposit in the 'as deposited' condition for (a.1, a.2, c.1) AA5083 and (b.1, b.2, c.2) AA7050 MLFS interlayer structures.

depositing onto an AA2050 substrate directly, justifying the need for an FS interlayer structure.

3.2. Investigation of MLFS deposited material (without WAAM)

The deposition of multi-layer AA5083 FS structures onto AA2050 substrate has already been investigated in depth in previous studies [30, 31] and is presented here only for completeness, see Figs. 6(a) and 9a. Consistently high values in strength along the MLFS stacks and a homogeneous hardness along the build direction can be noticed.

For AA7050, the hardness mapping shows a hardness increase towards the top layer, Fig. 10b. In contrast to AA5083, AA7050 is a precipitation-hardenable alloy and the subsequent FS layer depositions introduce additional thermo-mechanical input, affecting the layers already deposited, i.e., causing dissolution of the precipitates. In this regard, the hardness is characteristic for MLFS deposition of precipitation hardenable aluminium alloys [44,45]. Furthermore, the substrate of the AA7050 MLFS stack shows a larger heat-affected zone (HAZ), which is a result of the higher process temperatures due to the higher axial force compared to AA5083 consumable material. In terms of the MFTT results, Fig. 6(b), the AA7050/AA2050 material combination presents consistent results in terms of $R_{p0.2}$ along the stacks' length, where the results in terms of the ultimate tensile strength (UTS) show a larger scatter compared to the AA5083 MLFS stacks. However, the CTT results for the AA7050 MLFS stacks, which provide the testing of a 100×larger bonding area than the MFTT, show consistently high values along the AA7050 MLFS stacks. Overall, both consumable materials investigated achieved sufficient bonding to the AA20250 substrate material without defects, in contrast to the previously discussed WAAM process, i.e., WAAM deposit of AA5087 onto AA2050, Fig. 5.

3.3. Investigation of WAAM-MLFS deposit

Cross sections of the WAAM-MLFS structures on a AA2050 substrate with the WAAM part in the 'as deposited' condition is presented in Fig.

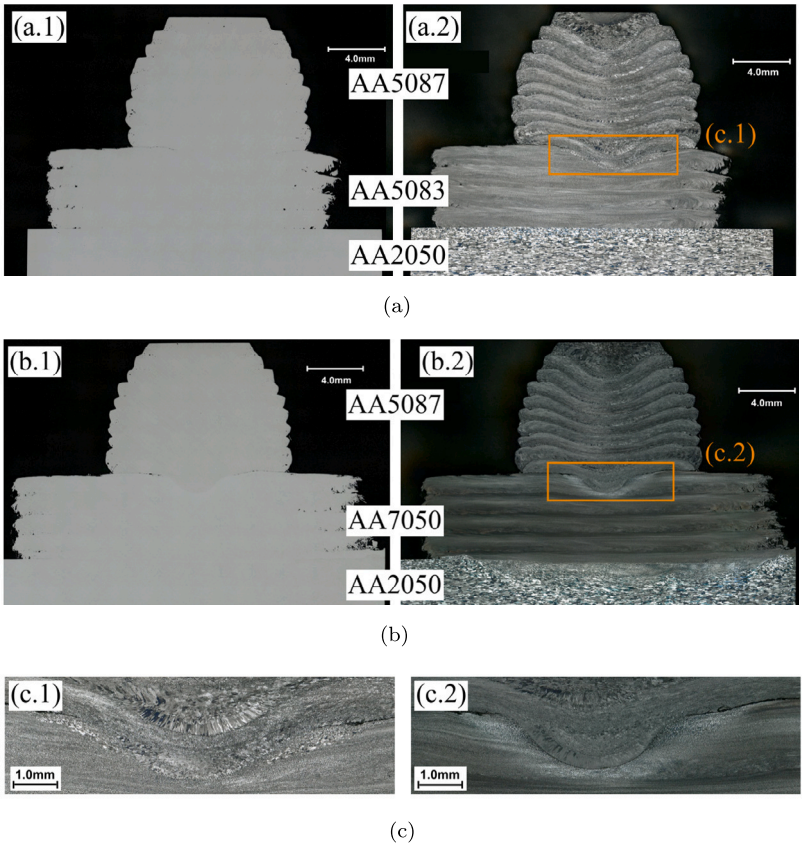

Fig. 8. Cross sections before and after etching for WAAM-MLFS structure on AA2050 substrate with inter-layer rolling applied for the WAAM deposit for (a.1, a.2, c.1) AA5083 and (b.1, b.2, c.2) AA7050 MLFS interlayer structures.

7. The AA5087 WAAM part shows distinct pores, commonly observed for aluminium WAAM deposits and previously reported in depth for this alloy [46]. For both MLFS interlayer structures from AA5083 and AA7050, the WAAM deposits indicate a sound bonding. Macrographs of the structures with inter-layer rolling of the WAAM part are shown in Fig. 8. When inter-layer rolling is applied to the WAAM deposits, the amount of pores is significantly decreased, as previously reported [46]. Furthermore, the inter-layer rolling leads to a WAAM deposit that is thinner and wider. From the etched cross sections in Figs. 7 and 8, it is observable that the grain size decreases with application of inter-layer rolling, which is consistent with the investigation by Gu et al. [32]. For more details on the underlying mechanisms, the reader is referred to [32], which are skipped in the context of this study for brevity.

The hardness measurement results for the stacks with AA5083 and AA7050 consumable stud material used for MLFS are shown in Figs. 9 and 10, respectively. In case of the AA5083 MLFS interlayer structure, the AA2050 substrate presents a characteristic hardness profile after MLFS in terms of local hardness value measured affected depth, Fig. 9, which is not further altered after WAAM or WAAM with inter-layer rolling. Since more MLFS layers are deposited for the reference case in comparison to the interlayer structures, the results indicate that the main thermo-mechanical effect on the substrate is occurring during the deposition of the first four MLFS layers.

The WAAM stack in the 'as deposited' condition, Fig. 9(b), has a homogeneous hardness within the MLFS as well as WAAM parts, which is in the range between 80 and 90 HV0.2. In contrast, the WAAM sample with inter-layer rolling at 45 kN, Fig. 9(c), has a continuous increase in hardness along the build direction, with a hardness of approx. 120 HV0.2 at the top of the stack, which is 10% higher than the value reported by Gu et al. [32]. The higher hardness for inter-layer rolling compared to the 'as deposited' WAAM condition can be related to the finer grains, deformation-induced high-density dislocations and sub-structures [32].

In contrast to 5xxx aluminium alloys, AA7050 is a precipitation-hardenable alloy, i.e., size and distribution of the precipitates are the major strengthening mechanism. For MLFS stacks, precipitation-hardenable alloys are known to have a continuous hardness increase towards the top layer, i.e., the layer that did not undergo subsequent thermo-mechanical processing cycles, Fig. 10(a). For the AA7050 MLFS stack with AA5087 WAAM layers on top in the 'as deposited' condition, shown in Fig. 10. Within the WAAM 'as deposited' part, Fig. 10(b), a homogeneous hardness similar to the WAAM sample 'as deposited' with AA5083 MLFS consumable material, Fig. 9(b), is observed. The WAAM part for the sample with inter-layer rolling, Fig. 10(c), has a similar profile compared to the sample with AA5083 MLFS consumable material, Fig. 9(c), with no significant effect on the AA7050 MLFS interlayer structure. The results of the AA7050 MLFS interlayer structure with inter-layer rolling indicate that the precipitates, which are the major strengthening mechanism of this alloy, are not significantly affected. As discussed above, the AA5083 showed an effect of inter-layer rolling for WAAM on the hardness. For this alloy, the grain size is crucial for the hardness, indicating that a slight refinement in grain size might have occurred leading to slight hardness increases in some parts of the MLFS deposit.

For both WAAM conditions, 'as deposited' and with inter-layer rolling, there is a drop of hardness at the interface between AA5087 WAAM material and AA7050 MLFS. Overall, the inter-layer rolling leads to an increased hardness for AA5087 WAAM deposit. For the substrate material, no distinct influence could be observed comparing WAAM 'as deposited' and with inter-layer rolling.

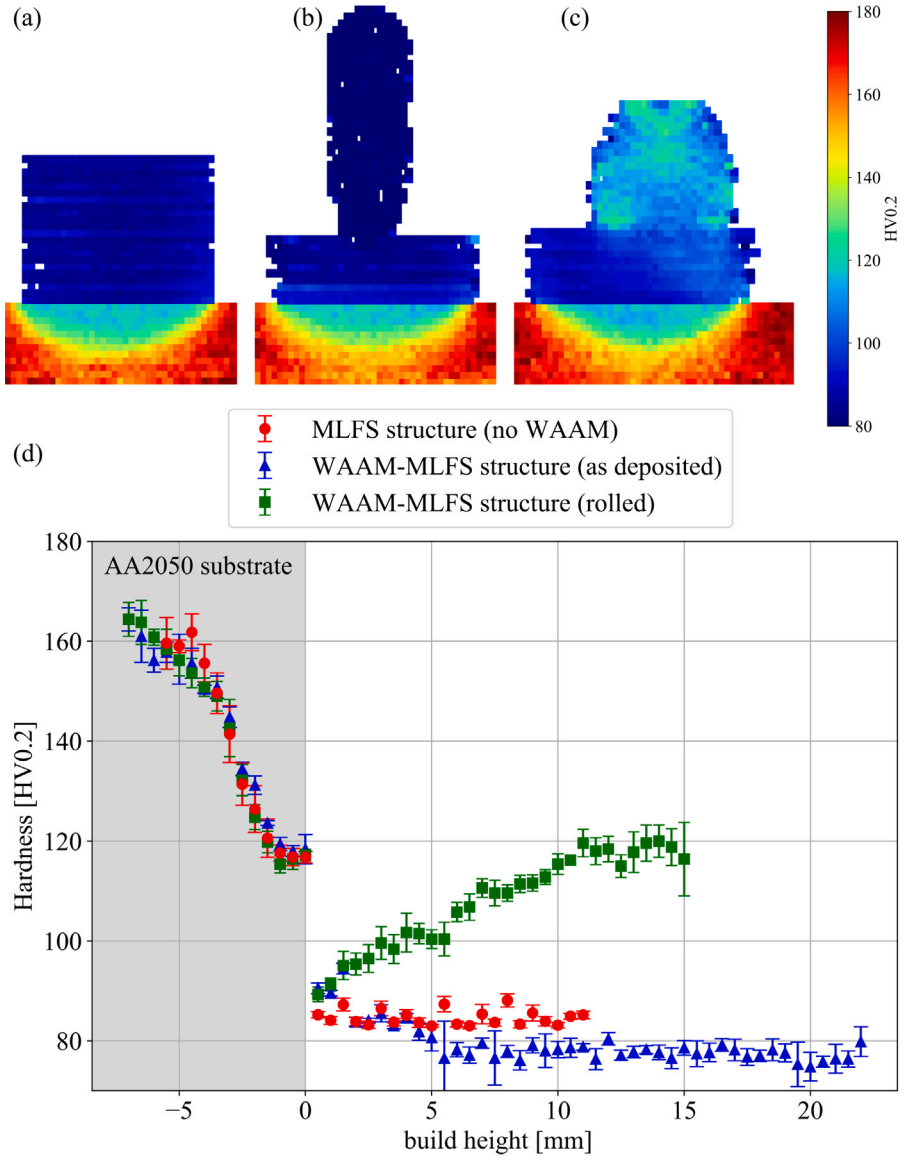

Fig. 9. Hardness mapping results for (a) MLFS stack (9 layers, AA5083), (b) MLFS (4 layers, AA5083)-WAAM (10 layers, AA5087) stack 'as deposited', (c) MLFS (4 layers, AA5083)-WAAM (10 layers, AA5087) stack with inter-layer rolling and (d) average hardness along build direction for five lines in the centre of the respective stacks.

Table 4
Yield strength, ultimate tensile strength and elongation obtained for MFTT with specimens taken from WAAM-MLFS interface.

MLFS alloy	WAAM deposit condition	Yield strength [MPa]	UTS [MPa]	Elongation at fracture [%]
AA5083	As-deposited	169.50 ± 3.83	247.52 ± 11.94	30.20 ± 3.88
AA5083	Rolled	251.83 ± 29.46	273.87 ± 44.43	18.31 ± 8.48
AA7050	As-deposited	201.00 ± 3.16	272.07 ± 8.13	25.36 ± 2.65
AA7050	Rolled	267.40 ± 16.61	291.54 ± 27.73	18.07 ± 7.38
AA5083 WAAM-as deposited [32]		142	291	22.4
AA5083 WAAM-as rolled [32]		239	355	20.1

The results obtained from MFTT[1] with specimens extracted from the WAAM-MLFS interface are presented in Table 4 and underline the effect of the inter-layer rolling. The mechanical properties of the AA5087 WAAM on AA5083 MLFS interface are significantly improved when inter-layer rolling is applied, increasing the yield strength and the ultimate tensile strength compared to the structure with the 'as deposited' WAAM condition, Table 4. On the other hand, elongation is reduced. For the AA5087 WAAM on AA7050 MLFS interface, the inter-layer rolling results in an increase of the yield strength and ultimate tensile strength while the elongation is reduced compared to the respective structure 'as deposited' WAAM condition, Table 4.

The yield strength values obtained here for both 'as deposited' and with inter-layer rolling are comparable to those obtained in the work of Gu et al. [32] for WAAM AA5087 on AA5083, however, their

[1] The data recorded by the testing equipment, i.e., stress-strain curves for the individual specimens, is presented in Appendix.

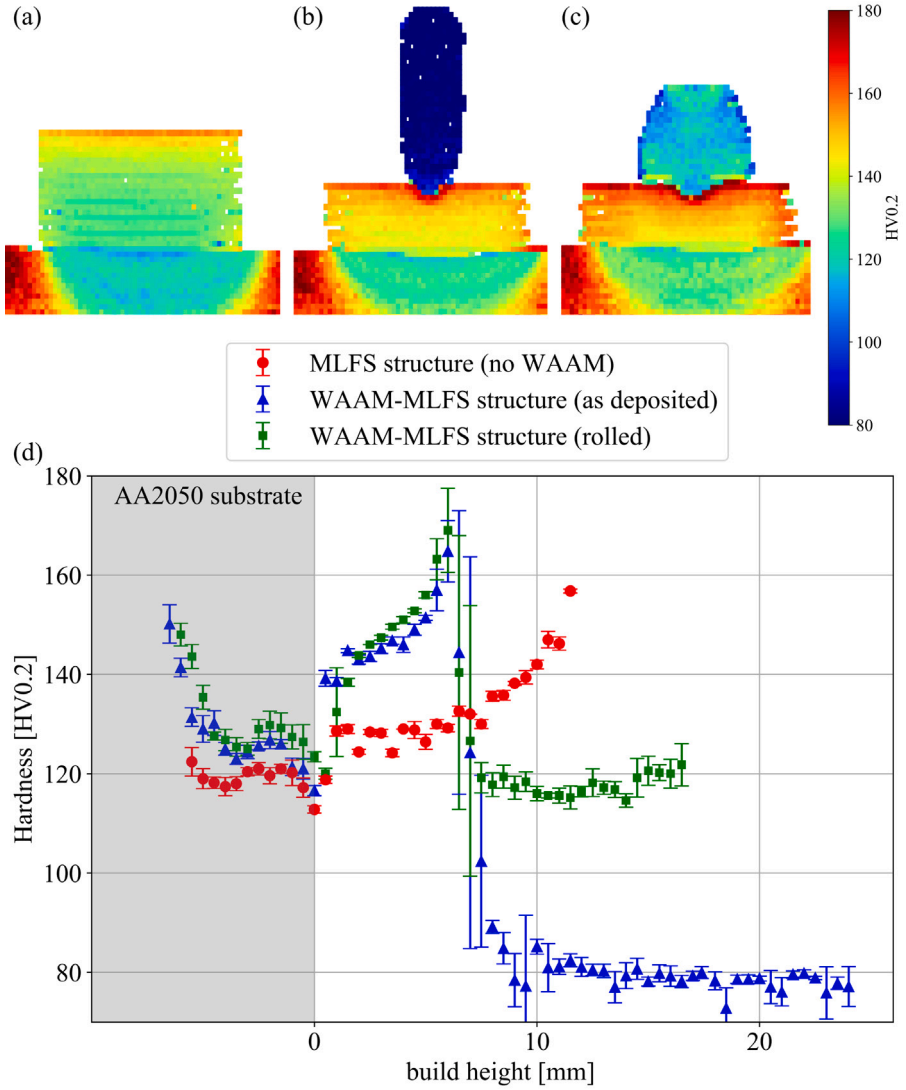

Fig. 10. Hardness mapping results for (a) MLFS stack (9 layers, AA7050) [31], (b) MLFS (5 layers, AA5083)-WAAM (10 layers, AA5087) stack 'as deposited', (c) MLFS (5 layers, AA7050)-WAAM (10 layers, AA5087) stack with inter-layer rolling and (d) average hardness along build direction for five lines in the centre of the respective stacks.

reported UTS values were significantly higher. When the high-strength AA7050 aluminium alloy is used as MLFS consumable material, yield strength and UTS obtained from the MFTT are higher compared to structures with AA5083, where the yield strength is overmatching the values reported by Gu et al. [32]. Comparing the results, it has to be mentioned that Gu et al. [32] investigated significantly larger specimens containing multiple WAAM layers and their interfaces. The MFTT results presented in this study were obtained with specimens extracted from the WAAM-MLFS interface, containing the fusion zone, Fig. 4.

Comparing the MFTT results for the MLFS-substrate interface and the WAAM-MLFS interface, the UTS values obtained for at the interface of MLFS layer-to-substrate is overmatching the values obtained for the WAAM-MLFS interface specimens, see Fig. 6 and Table 4. This might indicate a stronger bonding of the MLFS deposit to the substrate compared to the WAAAM-to-MLFS bonding. In terms of $R_{p0.2}$, the yield strength, the results for MLFS-substrate interface specimens are comparable to WAAM-MLFS specimens results in the 'as deposited' condition. As already mentioned, the inter-layer rolling leads to very high yield strength for the 5xxx aluminium alloy. For the AA7050 MLFS consumable material, the MLFS-substrate specimens presented a yield strength comparable to the WAAM-MLFS specimens with inter-layer rolling.

Overall, the results obtained highlight that sound bonding is achievable between WAAM and previously deposited MLFS structures. AA7050 MLFS produces a joint that performs higher than the WAAM deposit, enabling the use of the AA2050 substrate and AA5087 WAAM combination. The application of inter-layer rolling improves the mechanical properties of the overall structure.

4. Summary and conclusions

The presented work highlights that combining solid-state and fusion-based AM techniques can be an appealing approach to build hybrid structures, exploiting the advantages of a solid-state layer deposition approach to achieve a material combination that is challenging for fusion-based processes. Two different aluminium alloys were used as consumable materials to build the interlayer structure via MLFS. Additionally, the effect of inter-layer rolling was investigated on the following WAAM deposit. Hybrid structures build from three different aluminium alloys were investigated. The main findings can be summarized as follows:

- Both, AA5083 and AA7050 MLFS deposited structures, are feasible alloys for interlayer structures between AA2050 substrate and AA5087 WAAM deposit.

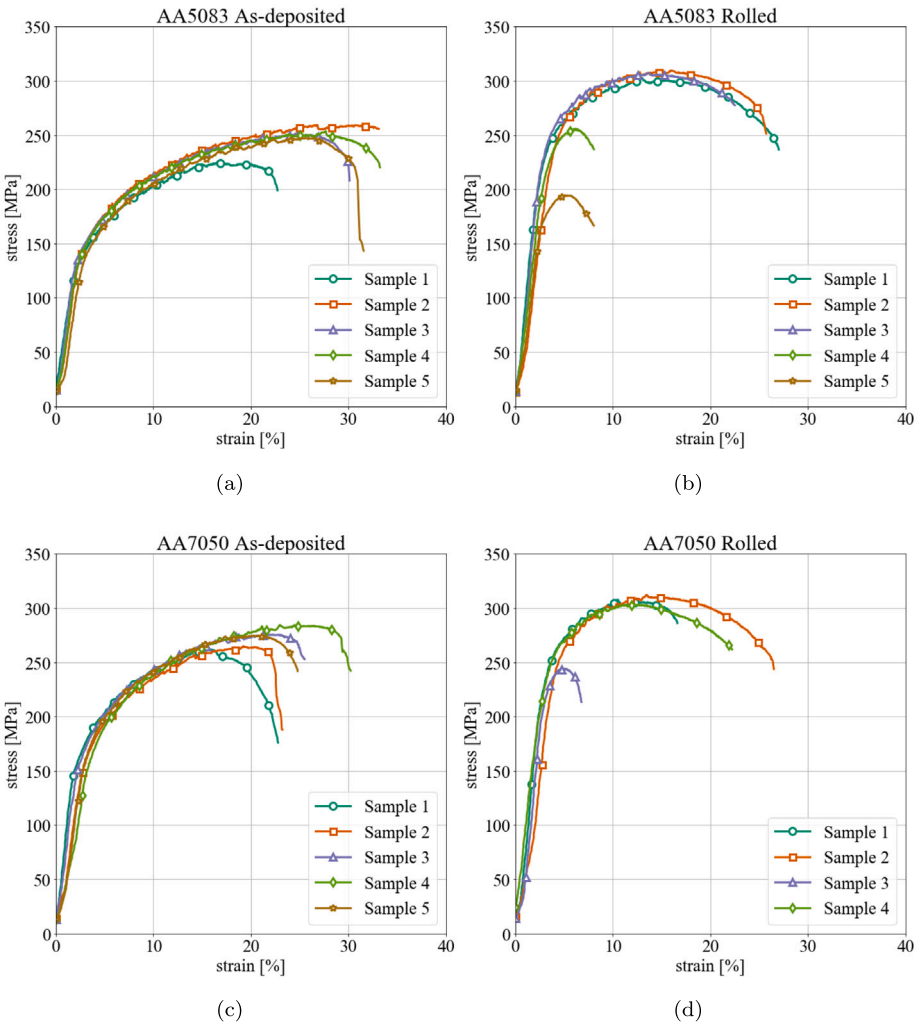

Fig. A.11. Stress–strain curves for all tensile specimens taken from the WAAM-MLFS interface (Fig. 4) for MLFS consumable material of (a) AA5083 with WAAM 'as deposited', (b) AA5083 with WAAM with inter-layer rolling, (c) AA7050 with WAAM 'as deposited' and (d) AA7050 with WAAM with inter-layer rolling.

- The implementation of the AA7050 MLFS interlayer structure led to a graded interface with improved properties compared to the WAAM deposit, enabling this structure to be used for application.
- The investigation of the tensile strength at the interfaces of the hybrid structures revealed that both interfaces (MLFS-substrate and WAAM-MLFS) present sound bonding. The inter-layer rolling is capable to significantly increase yield strength and ultimate tensile strength for both material combinations investigated in this work.
- The interlayer structure deposited via MLFS protected the substrate from re-heating during WAAM layer deposition.

The next steps in future research are the investigation of larger specimens to assess the overall performance of the hybrid MLFS-WAAM structures. Design application cases can also be explored to demonstrate the potential of this method to produce structural components.

CRediT authorship contribution statement

Zina Kallien: Writing – review & editing, Writing – original draft, Visualization, Validation, Methodology, Investigation, Formal analysis, Data curation, Conceptualization. **Eloise Eimer:** Writing – review & editing, Visualization, Validation, Methodology, Investigation, Formal analysis, Data curation, Conceptualization. **Arne Roos:** Writing – review & editing, Writing – original draft, Visualization, Validation, Methodology, Investigation, Formal analysis, Data curation, Conceptualization. **Victor Ortolland:** Writing – review & editing, Investigation. **Lars Rath:** Writing – review & editing, Validation, Methodology, Investigation, Formal analysis, Data curation. **Stewart Williams:** Writing – review & editing, Supervision, Resources, Funding acquisition. **Benjamin Klusemann:** Writing – review & editing, Supervision, Resources, Funding acquisition.

Funding

This research was partially funded by the European Union's Horizon 2020 research and innovation programmeunder grant agreement No 723600 through the LASIMM project.

Declaration of competing interest

The authors declare that they have no known competing financial interests or personal relationships that could have appeared to influence the work reported in this paper.

Appendix. Tensile testing results - WAAM-MLFS interface

The stress–strain curves for the individual MFTT specimens tested for both MLFS consumable materials as well as both WAAM conditions are presented in Fig. A.11. The data underlines the significant improvement of the WAAM-MLFS interface when inter-layer rolling is applied during DED layer deposition.

Data availability

Data will be made available on request.

References

[1] N. Khan, A. Riccio, A systematic review of design for additive manufacturing of aerospace lattice structures: Current trends and future directions, Prog. Aerosp. Sci. 149 (2024) http://dx.doi.org/10.1016/j.paerosci.2024.101021.

[2] D. Herzog, V. Seyda, E. Wycisk, C. Emmelmann, Additive manufacturing of metals, Acta Mater. 117 (2016) 371–392, http://dx.doi.org/10.1016/j.actamat.2016.07.019.

[3] L.E. Murr, S.M. Gaytan, D.A. Ramirez, E. Martinez, J. Hernandez, K.N. Amato, P.W. Shindo, F.R. Medina, R.B. Wicker, Metal fabrication by additive manufacturing using laser and electron beam melting technologies, J. Mater. Sci. Technol. 28 (1) (2012) 1–14, http://dx.doi.org/10.1016/S1005-0302(12)60016-4.

[4] N. Prasad, A.G. Eswara, R.J.H. Wanhill (Eds.), Aluminum-Lithium Alloys: Processing, Properties, and Applications, Butterworth-Heinemann, ISBN: 978-0-12-401698-9, 2014.

[5] Z. Sun, W. Shao, B. He, H. Wang, Achieving fully equiaxed grains with minor Sc addition of a novel Al-Li alloy fabricated by laser direct energy deposition, Mater. Lett. 370 (2024) http://dx.doi.org/10.1016/j.matlet.2024.136780.

[6] Y. Sun, H. Liu, C. Wu, Y. Liu, R. Xie, Z. Wang, Y. Han, S. Chen, Effect of the aging process on the precipitated phase of 2195 Al-Li alloy deposited by preheating and water-cooling assisted friction rolling additive manufacturing, J. Alloys Compd. 1022 (2025) http://dx.doi.org/10.1016/j.jallcom.2025.179826.

[7] M. Roscher, Z. Sun, E.A. Jägle, Designing Al alloys for laser powder bed fusion via laser surface melting: Microstructure and processability of 7034 and modified 2065, J. Mater. Process. Technol. 326 (2024) http://dx.doi.org/10.1016/j.jmatprotec.2024.118334.

[8] E. Eimer, J. Ding, S. Williams, From wire to component: Aluminium lithium alloy development for wire and arc additive manufacturing, BHM Berg- Hüttenmänn. Mon.hefte 169 (1) (2024) 9–16, http://dx.doi.org/10.1007/s00501-023-01417-5.

[9] M. Merklein, R. Schulte, T. Papke, An innovative process combination of additive manufacturing and sheet bulk metal forming for manufacturing a functional hybrid part, J. Mater. Process. Technol. 291 (2021) 117032, http://dx.doi.org/10.1016/j.jmatprotec.2020.117032.

[10] G. Ambrogio, F. Gagliardi, M. Muzzupappa, L. Filice, Additive-incremental forming hybrid manufacturing technique to improve customised part performance, J. Manuf. Process. 37 (2019) 386–391, http://dx.doi.org/10.1016/j.jmapro.2018.12.008.

[11] M. Bambach, I. Sizova, B. Sydow, S. Hemes, F. Meiners, Hybrid manufacturing of components from Ti-6Al-4V by metal forming and wire-arc additive manufacturing, J. Mater. Process. Technol. 282 (2020) 116689, http://dx.doi.org/10.1016/j.jmatprotec.2020.116689.

[12] S.W. Williams, F. Martina, A.C. Addison, J. Ding, G. Pardal, P. Colegrove, Wire + arc additive manufacturing, Mater. Sci. Technol. 32 (7) (2016) 641–647, http://dx.doi.org/10.1179/1743284715Y.0000000073.

[13] E. Eimer, S. Williams, J. Ding, S. Ganguly, B. Chehab, Effect of substrate alloy type on the microstructure of the substrate and deposited material interface in aluminium wire + arc additive manufacturing, Metals 11 (2021) 916, http://dx.doi.org/10.3390/met11060916.

[14] E. Eimer, S. Williams, J. Ding, S. Ganguly, B. Chehab, Mechanical performances of the interface between the substrate and deposited material in aluminium wire direct energy deposition, Mater. Des. 225 (2023) 111589, http://dx.doi.org/10.1016/j.matdes.2023.111594.

[15] J. Zhang, X. Zhang, X. Wang, J. Ding, Y. Traoré, S. Paddea, S. Williams, Crack path selection at the interface of wrought and wire+arc additive manufactured Ti–6Al–4V, Mater. Des. 104 (2016) 365–375, http://dx.doi.org/10.1016/j.matdes.2016.05.027.

[16] N.Eswara Prasad, Amol A. Gokhale, R.J.H. Wanhill, Aluminum-Lithium Alloys - Processing, Properties, and Applications, Elsevier, ISBN: 978-0-12-401698-9, 2014.

[17] I.N. Fridlyander, T.I. Malinkina, N.V. Shiryaeva, I.F. Anokhin, T.A. Gorokhova, Properties of welded joints in alloy 01420, Met. Sci. Heat Treat. (17) (1975) http://dx.doi.org/10.1007/BF00663692.

[18] Miroslav Sahul, Martin Sahul, Michaela Kritikos, Maroš Vyskoč, The effect of electron beam oscillation on the porosity of third-generation AW2099 aluminium lithium alloy welded joints, Mater. Lett. 339 (2023) 134093, http://dx.doi.org/10.1016/j.matlet.2023.134093.

[19] Harpreet Sidhar, Nelson Y. Martinez, Rajiv S. Mishra, Juergen Silvanus, Friction stir welding of Al–Mg–Li 1424 alloy, Mater. Des. 106 (2016) http://dx.doi.org/10.1016/j.matdes.2016.05.111.

[20] Ho-Sung Lee, Jong-Hoon Yoon, Joon-Tae Yoo, Kookil No, Friction stir welding process of aluminum-lithium alloy 2195, Procedia Eng. 149 (2016) http://dx.doi.org/10.1016/j.proeng.2016.06.639.

[21] X. Guo, D. Ni, H. Li, P. Xue, R. Xu, Z. Pan, S. Zhou, Z. Ma, Enhancing strength, ductility, and fatigue performance of Al-Zn-Mg-Cu-Sc-Zr alloy using a hybrid approach: wire-arc directed energy deposition and interlayer friction stir processing, J. Mater. Process. Technol. 322 (2023) 118173, http://dx.doi.org/10.1016/j.jmatprotec.2023.118173.

[22] R. Mishra, D. Pandit, M. Imam, Microstructure, mechanical and corrosion study of friction stir processed Inconel 625 additive layers deposited via wire arc direct energy deposition, Addit. Manuf. 86 (2024) 104193, http://dx.doi.org/10.1016/j.addma.2024.104193.

[23] V. Fitseva, S. Hanke, J.F. dos Santos, P. Stemmer, B. Gleising, The role of process temperature and rotational speed in the microstructure evolution of Ti-6Al-4V friction surfacing coatings, Mater. Des. 110/15 (2016) 112–123, http://dx.doi.org/10.1016/j.matdes.2016.07.132.

[24] J.C. Galvis, P.H.F. Oliveira, J.d.P. Martins, A.L.M.d. Carvalho, Assessment of process parameters by friction surfacing on the double layer deposition, Mater. Res. 21 (3) (2018) 321, http://dx.doi.org/10.1590/1980-5373-mr-2018-0051.

[25] R. Damodaram, P. Rai, S. Cyril Joseph Daniel, R. Bauri, D. Yadav, Friction surfacing: A tool for surface crack repair, Surf. Coat. Technol. 422 (2021) 127482, http://dx.doi.org/10.1016/j.surfcoat.2021.127482.

[26] D. Guo, C.T. Kwok, S.L.I. Chan, Spindle speed in friction surfacing of 316L stainless steel – How it affects the microstructure, hardness and pitting corrosion resistance, Surf. Coat. Technol. 361 (2019) 324–341, http://dx.doi.org/10.1016/j.surfcoat.2019.01.055.

[27] H. Li, W. Qin, A. Galloway, A. Toumpis, Friction surfacing of aluminium alloy 5083 on DH36 steel plate, Metals 9 (2019) 479, http://dx.doi.org/10.3390/met9040479.

[28] S. Palanivel, R.S. Mishra, Building without melting: a short review of friction-based additive manufacturing techniques, Int. J. Addit. Subtract. Mater. Manuf. 1 (1) (2017) 82–103.

[29] D.D. Lu, J.F. Li, H. Ning, P.C. Ma, Y.L. Chen, X.H. Zhang, K. Zhang, J.M. Li, R.F. Zhang, Effects of microstructure on tensile properties of AA2050-T84 Al-Li alloy, Trans. Nonferr. Met. Soc. China 31 (5) (2021) 1189–1204, http://dx.doi.org/10.1016/S1003-6326(21)65571-1.

[30] M. Soujon, Z. Kallien, A. Roos, B. Zeller-Plumhoff, B. Klusemann, Fundamental study of multi-track friction surfacing deposits for dissimilar aluminum alloys with application to additive manufacturing, Mater. Des. 219 (2022) 110786, http://dx.doi.org/10.1016/j.matdes.2022.110786.

[31] L. Rath, Z. Kallien, A. Roos, J. dos Santos, B. Klusemann, Anisotropy and mechanical properties of dissimilar Al additive manufactured structures generated by multi-layer friction surfacing, Int. J. Adv. Manuf. Technol. 125 (2023) 2091–2102, http://dx.doi.org/10.1007/s00170-022-10685-3.

[32] J. Gu, X. Wang, J. Bai, J. Ding, S. Williams, Y. Zhai, K. Liu, Deformation microstructures and strengthening mechanisms for the wire+arc additively manufactured Al-Mg4.5Mn alloy with inter-layer rolling, Mater. Sci. Eng. A 712 (2018) 292–301, http://dx.doi.org/10.1016/j.msea.2017.11.113.

[33] H. Klopstock, A.R. Neelands, An improved method of joining or welding metals, 1941.

[34] J.Q. Li, T. Shinoda, Underwater friction surfacing, Surf. Eng. 16/1 (2000) 31–35, http://dx.doi.org/10.1179/026708400322911483.

[35] K. Fukakusa, On the characteristics of the rotational contact plane - a fundamental study of friction surfacing, Weld. Int. 10/7 (1996) 524–529, http://dx.doi.org/10.1080/09507119609549043.

[36] X.M. Liu, Z.D. Zou, S.Y. Zhang, S.Y. Qu, X.H. Wang, Transferring mechanism of the coating rod in friction surfacing, Surf. Coat. Technol. 202/9 (2008) 1889–1894, http://dx.doi.org/10.1016/j.surfcoat.2007.08.024.

[37] S. Hanke, J.F. Dos Santos, Comparative study of severe plastic deformation at elevated temperatures of two aluminium alloys during friction surfacing, J. Mater. Process. Technol. 247 (2017) 257–267, http://dx.doi.org/10.1016/j.jmatprotec.2017.04.021.

[38] J. Gandra, H. Krohn, R.M. Miranda, P. Vilaça, L. Quintino, J.F. Dos Santos, Friction surfacing - A review, J. Mater. Process. Technol. 214/5 (2014) 1062–1093, http://dx.doi.org/10.1016/j.jmatprotec.2013.12.008.

[39] Federation of European producers of abrasives, FEPA P 43-D-1984: P-grit sizes coated, Diamond abrasives, Paris, France, 1993.

[40] H. Sakihama, H. Tokisue, K. Katoh, Mechanical properties of friction surfaced 5052 aluminum alloy, Mater. Trans. 44 (12) (2003) 2688–2694, http://dx.doi.org/10.2320/matertrans.44.2688.

[41] C. Huang, S. Kou, Partially melted zone in aluminum welds – liquation mechanism and directional solidification, Weld. J. 79 (2000).

[42] L. Hong, Y. Weian, L. Zhuoxin, M. Bober, S. Jacek, Z. Yu, Numerical and experimental study of the hot cracking phenomena in 6061/7075 dissimilar aluminum alloy resistance spot welding, J. Manuf. Process. 77 (2022) 794–808, http://dx.doi.org/10.1016/j.jmapro.2022.04.001.

[43] C. Huang, G. Cao, S. Kou, Liquation cracking in partial penetration aluminium welds: assessing tendencies to liquate, crack and backfill, Sci. Technol. Weld. Join. 9 (2004) 149–157, http://dx.doi.org/10.1179/136217104225017071.

[44] J. Gandra, P. Vigarinho, D. Pereira, R.M. Miranda, A. Velhinho, P. Vilaça, Wear characterization of functionally graded Al–SiC composite coatings produced by friction surfacing, Mater. Des. 52 (2013) 373–383, http://dx.doi.org/10.1016/j.matdes.2013.05.059.

[45] J. Vivas, M. Roldán, L. García-Sesma, M. Chludzinski, O. Zubiri, E. Aldanondo, Fundamental study on multi-layer friction surfacing of 2017 aluminum alloy on 6082 aluminum alloy, Prog. Addit. Manuf. (2024) http://dx.doi.org/10.1007/s40964-024-00834-3.

[46] J. Gu, J. Ding, S.W. Williams, H. Gu, P. Ma, Y. Zhai, The effect of inter-layer cold working and post-deposition heat treatment on porosity in additively manufactured aluminum alloys, J. Mater. Process. Technol. 230 (2016) 26–34, http://dx.doi.org/10.1016/j.jmatprotec.2015.11.006.